JACS
JOURNAL OF THE AMERICAN CHEMICAL SOCIETY

ARTICLE

pubs.acs.org/JACS

The Fragmentation−Recombination Mechanism of the Enzyme Glutamate Mutase Studied by QM/MM Simulations

Judith B. Rommel and Johannes Kästner*

Computational Biochemistry Group, Institute of Theoretical Chemistry, University of Stuttgart, Stuttgart, Germany

Supporting Information

ABSTRACT: The radical mechanism of the conversion of glutamate to methylaspartate catalyzed by glutamate mutase is studied with quantum mechanical/molecular mechanical (QM/MM) simulations based on density functional theory (DFT/MM). The hydrogen transfer between the substrate and the cofactor is found to be rate limiting with a barrier of 101.1 kJ mol^{-1}. A careful comparison to the uncatalyzed reaction in water is performed. The protein influences the reaction predominantly electrostatically and to a lesser degree sterically. Our calculations shed light on the atomistic details of the reaction mechanism. The well-known arginine claw and Glu 171 (*Clostridium cochlearium* notation) are found to have the strongest influence on the reaction. However, a catalytic role of Glu 214, Lys 322, Gln 147, Glu 330, Lys 326, and Met 294 is found as well. The arginine claw keeps the intermediates in place and is probably responsible for the enantioselectivity. Glu 171 temporarily accepts a proton from the glutamyl radical intermediate and donates it back at the end of the reaction. We relate our results to experimental data when available. Our simulations lead to further understanding of how glutamate mutase catalyzes the carbon skeleton rearrangement of glutamate.

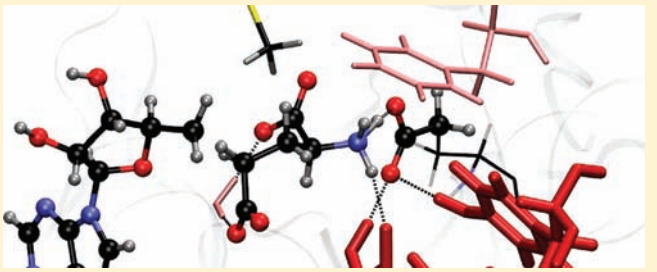

1. INTRODUCTION

Catalysts for radical reactions are important in industrial processes. The understanding of enzymes catalyzing radical reactions allows to design new biomimetic catalysts. Computational investigations complemented by experiments can provide better insight into the use and the control of radicals by biological systems.

Adenosylcobalamin-dependent glutamate mutase (GM) belongs to a group of enzymes that catalyze radical reactions and use adenosylcobalamin (coenzyme B_{12}) as a cofactor.[1] GM occurs as a tetramer consisting of two identical $\sigma\varepsilon$-dimers each made up of a σ-subunit and an ε-subunit. One cofactor is bound to each $\sigma\varepsilon$-interface. GM is found in anaerobic bacteria, e.g. in *Clostridium spec.*[2] They use glutamate as a carbon and energy source and degrade it to butyrate, CO_2, NH_4^+, and H_2.[3] This work focuses on the first step of glutamate fermentation by those bacteria which starts with a reversible interconversion including a carbon-skeleton rearrangement of (*S*)-glutamate to (2*S*,3*S*)-3-methylaspartate (MA, see Figure 1). This reaction involves radical intermediates. Both, the substrate and the product are small, stable molecules. The reaction is reversible. Thus, glutamate mutase provides a relatively simple system to study enzymatic catalysis using radicals.

The crystal structure of the enzyme in complex with substrate and cofactor has been determined at 1.6 and 1.9 Å resolution.[4,5] NMR structures are available as well.[6−9] Key residues in the vicinity of the active site of GM are, e.g., Arg 149, Arg 100, and Arg 66, which form hydrogen bonds to the glutamate substrate. They establish the so-called arginine 'claw'.[4] Glu 171 was suggested to act as a a proton acceptor during the reaction.[10] Here and in the following residue numbers refer to GM from *Clostridium cochlearium*.

According to the bound free-radical hypothesis, the initial step in coenzyme B12-mediated reactions is the homolytic cleavage of the cobalt−carbon bond of the cofactor, which produces a 5′-desoxyadenosyl radical (Ado) and cob(II)alamin.[11,12] Compared to the following hydrogen transitions catalyzed by GM, the homolytic cleavage is fast; it is not rate limiting.[13−15] Therefore it is not considered in our simulations.

Several reaction mechanisms have been proposed, e.g., removal of a hydride ion or a not very likely addition−elimination pathway.[16] We study the fragmentation−recombination mechanism proposed based on experimental data.[17,18] In this mechanism the homolytic cleavage is followed by the transfer of the unpaired electron from Ado to the glutamate substrate. After the rearrangement to a methylaspartyl radical, the unpaired electron is transferred back to Ado (see Figure 1). These steps are rate limiting and are investigated in this study. The final part of the catalysis is reformation of the Co−C bond and product release.

From experiment, it is unclear which of the individual steps is rate limiting. While some studies observed large H/D KIEs,[19−21] which indicate the hydrogen-transfer steps to be rate limiting,

Received: March 14, 2011
Published: May 25, 2011

dx.doi.org/10.1021/ja202312d | *J. Am. Chem. Soc.* 2011, 133, 10195–10203

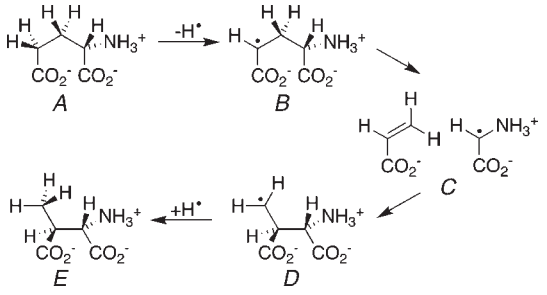

Figure 1. The rearrangement of glutamate to methylaspartate catalyzed by GM: (A) Ado and glutamate; (B) Ado + H and glutamyl radical; (C) Ado + H, acrylate, and glycyl radical; (D) Ado + H and methylaspartyl radical; and (E) Ado and methylaspartate.

more recent work found smaller KIEs and concludes that neither of the hydrogen-transfer steps is cleanly rate limiting.[22,23]

A promising method to simulate enzymatic reactions is the combination of quantum chemical approaches and empiric force fields (QM/MM),[24,25] recently reviewed in references.[26−30] All previous QM/MM calculations performed on GM considered only the activating, but not rate limiting, Co−C bond cleavage.[13−15] The dissociation enthalpy for the homolytic cleavage was experimentally estimated in methylmalonyl-CoA mutase (MMCM), a similar coenzyme B_{12}-dependent enzyme, to be about 59 kJ mol^{-1}.[31] Calculations investigating the rearrangement reaction have been done in gas-phase models considering different protonation states.[16,32] MMCM has been investigated with QM/MM and other computational methods.[33−35] Both GM[21] and MMCM[36] generate a carbon-centered substrate radical after the homolytic Co−C bond cleavage. The cofactor−substrate arrangement of MMCM resembles that of GM.[37] Nevertheless, computational studies[35] favor an addition−elimination mechanism for MMCM, whereas for GM experimental as well as computational results support the fragmentation−recombination pathway.[16]

The paper is organized as follows: In the Section II methodological details and the level of theory are given. In Section III our results concerning the energetics of the rearrangement reaction catalyzed by the enzyme are discussed. Then a detailed discussion of the enzyme environment and its influence on the reaction follows. Emphasis is given on individual amino acids and their contribution to a productive catalysis. To our knowledge this is the first study of the reaction mechanism of GM with the QM/MM approach.

2. METHODS

2.1. System Preparation. The enzyme GM from *C. cochlearium* in complex with 5′-desoxyadenosylcobalamin and substrate was modeled on X-ray diffraction results at 1.9 Å resolution (PDB entry 1I9C).[5] The X-ray data include the whole tetramer with two $\sigma\varepsilon$-subunits, and the substrate glutamate as well as (2*S*,3*S*)-3-methylaspartate. The enzyme consists of two identical subunits without any covalent connections between them. The reactive parts are remote from each other. Experimental investigations carried out with a mutant containing only one $\sigma\varepsilon$-subunit also show independence of the subunits.[38] Thus, we simulated only one $\sigma\varepsilon$-subunit.

After protonation and solvatization (both with VMD[39] version 1.8.7) in a cubic box of TIP3P[40] water molecules, the system was extensively equilibrated on an MM-only level. This allows all cavities within the enzyme to be filled with water. $Na^+$and Cl^- ions (each about 0.05 mol L^{-1}) were added to ensure an overall charge neutrality of the system. The initial size of the rectangular solvent box was 90.5 × 80.5 × 95 $Å^3$.

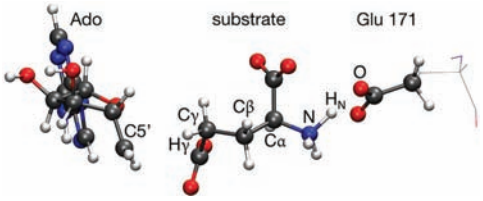

Figure 2. The QM region (in ball and stick representation) containing Ado (left), glutamate substrate (middle), and the side chain of Glu 171 (right). Carbon is shown in gray, oxygen in red, hydrogen in white, and nitrogen in blue. Atoms mentioned in the text are labeled.

In the following classical MD simulations with periodic boundary conditions were performed using the CHARMM22[41−44] force field in the code NAMD version 2.6.[45] The Langevin piston Nosé−Hoover method[46,47] was used to keep the system at 300 K and 1 bar. The time step was 2 fs. In the equilibration phase, constraints followed by position restraints by springs were applied to the whole protein, the cofactor, and the substrate. All water molecules, also those contained in the crystal structure, were unrestrained. The volume was kept constant in the equilibration. At first the solute atoms were completely frozen for 2000 conjugate gradient optimization steps and 0.1 ns of MD simulation. Next, restraints with a force constant of 5.0 kcal mol^{-1} $Å^{-2}$ were applied to the solute again for 2000 optimization steps and 0.1 ns of MD simulation. This was followed by 0.1 ns of MD simulation each with force constants of 2.0 and 0.1 kcal mol^{-1} $Å^{-2}$ to gradually relax the protein with the cofactor and the substrate. In one run the binding pocket of the enzyme contained the glutamate substrate (50 ns of sampling). Another run was performed for 26 ns for GM containing the product MA in the binding pocket.

For the MD run with glutamate in the binding pocket, the protein in solvent comprised 63 411 atoms, including 17 899 water molecules and 50 $Na^+$and Cl^- ions. Snapshots were taken from that MD run after 9, 20, 41, 32, 13, and 25 ns of simulation as initial structures for the following QM/MM calculations. They are labeled as SN-Glu-1 to SN-Glu-6. Three snapshots were taken from the MD simulation with MA in the binding pocket (SN-MA-1 to SN-MA-3) after 6, 11, and 15 ns. They served as starting configurations for the following geometry optimizations and transition-state searches. Force field parameters for nonstandard residues (cobalamin and MA) were derived by analogy to similar parametrized residues. They can be found in the Supporting Information. For the adenosyl part of coenzyme B_{12}, which is completely contained in the QM-part, we used the standard adenosyl parameters with the phosphate group deleted. The snapshots were chosen to cover a range of different C−C distances (from 3.2 to 5.12 Å) for the hydrogen-transfer reaction between the substrate and the cofactor.

To prepare the snapshots for simulation, all nonprotein atoms having a distance greater than 17 Å from the oxygen atom in the ribose ring of Ado were deleted from the model. This procedure removed the box of water except molecules in the inner part of the enzyme. During the calculations all residues that were entirely outside a range of 8 Å from any substrate or Ado atom were frozen. Additionally, all atoms of the adenosyl tail of cobalamin further away than 12 Å from Ado were frozen. That procedure resulted in 96−135 water molecules included in the different snapshots. Thus, all residues belonging to the first and second solvation shells of the environment of the active center were optimized. Additionally, in all snapshots except SN-Glu-1, 14 charged glutamate or aspartate residues on the surface of the protein were protonated to obtain a neutral system. All snapshots comprised about

10 200 atoms in the end. They contained water, protein, cofactor, and substrate but no $Na^+$and Cl^-ions from the solvatization.

2.2. QM Methods. Using QM/MM[24,25] geometry optimizations, the chemical steps of the reaction mechanism were investigated. The chemically active center was treated with DFT,[48,49] combined with the environment described by force field calculations. The QM/MM (potential energy) calculations were done with ChemShell,[26] using electrostatic embedding, where the MM charges of the force field polarize the QM part. Covalent bonds between the QM and MM parts were truncated on the QM side by hydrogen link atoms. The charge-shift scheme[26,50] was employed in order to avoid overpolarization of the QM density near the link. The CHARMM22 force field[41−44] in DL_POLY[51] as included in ChemShell[26] was used for the MM part.

Unless noted otherwise, the QM-region contained the glutamate substrate, Ado, and the side chain of Glu 171, see Figure 2. The truncation of the QM subsystem was done by cutting through the $C\beta-C\gamma$ bond of Glu 171. This resulted in a total of 54 QM atoms plus one hydrogen link atom. The choice of the truncation is well justified because only one single bond has been cut, and the distance between the cut and the chemically active atoms is three bonds at the minimum. Any possible charge transfer between the regions designated as QM and MM regions is neglected. In some calculations Glu 171 was left out (48 atoms) or His 150 was added (74 atoms) to the QM part to investigate specific effects. The homolytic cleavage in the cofactor is fast compared to the hydrogen transfer between Ado and glutamate substrate. Thus, cobalamin can be excluded from the QM part.

The QM part carries a charge of −2 and a spin multiplicity of 2. The QM region was described with DFT with BP86,[52−56] BP86-D,[57] and B3LYP[58] functionals as implemented in TURBOMOLE version 6.0.2.[59] The method of the resolution of the identity[60] was used throughout. Additionally, energies on the BP86-optimized geometry were calculated with the M06 functional[61] in NWChem version 5.1.1.[62,63]

Of the three functionals used, BP86, B3LYP, and M06, the latter can be expected to provide the most accurate results.[64] For technical reasons, calculations with the BP86 functional are much faster than calculations with the B3LYP functional, which are in turn faster than M06 calculations. Barriers are generally several kJ mol^{-1} higher with B3LYP and M06 than with BP86, which is in agreement with a generally observed trend caused by the Hartree−Fock exchange in B3LYP and M06 but not in BP86. M06 energies at BP86 geometries deviate only by about 1 kJ mol^{-1} from the M06 energies at B3LYP geometries, well within the error bar of QM/MM calculations. Thus, BP86 geometries were used.

After a comparison of def2-SVP,[65] cc-pVDZ,[66] def2-TZVP,[67] def2-TZVPP,[67] cc-pVTZ,[66] aug-cc-pVTZ,[66] cc-pVQZ,[66] and cc-pV5Z[66] basis sets (see Supporting Information), all computations were performed with the cc-pVTZ basis set, as larger basis sets led to insignificant changes in the energies. For cc-pVTZ calculations the number of SCF-basis functions was 1282.

The geometry optimizations were performed with DL-FIND[68] in ChemShell.[26] Hybrid delocalized internal coordinates (HDLC)[69] were used throughout.

Minima were located by a quasi-Newton limited memory Broyden−Fletcher−Goldfarb−Shanno (L-BFGS) method in ChemShell. This algorithm necessarily converges to minima, as we reverse the step, should it point uphill.[68]

Transition states were located with the superlinearly converging variant[70] of the dimer method.[71−73] Scans over bond lengths (for C−C-rearrangement steps) or bond-length differences (for hydrogen-transfer steps) were performed. All other degrees of freedom were relaxed. In each rearrangement step the two structures having the highest energies during the scans were chosen as a starting guess for the dimer calculations. The dimer method requires two initial structures. By construction it converges to first-order saddle points. Weights of 1 were used for all atoms in the QM part and weights of 0 for all other atoms in an algorithm described previously,[70] which effectively restricts the transition mode to the QM atoms. The energy is minimized with respect to the coordinates of all atoms with weight 0.

Table 1. Relative QM/MM Energies of Six Snapshots[a]

structure	SN-Glu-1	SN-Glu-2	SN-Glu-5
A	0.0	0.0	0.0
TS-**AB**	79.7	93.0	98.2
B	−21.6	−23.3	−29.7
TS-**BC**	61.3	56.7	51.9
C	21.7	40.7	14.5
TS-**CD**	70.9	78.5	46.1
D	9.2	7.6	−12.3
TS-**DE**	110.9	129.3	153.7
E	13.5	17.9	−1.5
structure	SN-MA-1	SN-MA-2	SN-MA-3
A	0.0	0.0	0.0
TS-**AB**	192.4	190.5	83.8
B	−37.0	−42.0	−36.9
TS-**BC**	38.9	43.5	43.9
C	−11.4	−19.2	−3.4
TS-**CD**	34.1	15.1	27.2
D	−26.1	−57.2	−49.6
TS-**DE**	110.2	140.1	60.7
E	−14.1	−51.3	−36.7

[a] M06 energies in kJ mol^{-1} at BP86 geometries.

To investigate the influence of the protein environment on the chemically active center, COSMO[74] calculations, which model a water environment, were performed in TURBOMOLE (default parameters for COSMO) for the glutamate substrate. Additionally, the isolated glutamate substrate was investigated in the gas phase.

To analyze the results of the optimizations, averages of the potential energy barriers of the snapshots were calculated by exponential averages:[75,76]

$$\langle \Delta E \rangle = -k_B T \ln\left\langle \exp\left(-\Delta E \frac{1}{k_B T}\right)\right\rangle \quad (1)$$

with T = 300 K, and k_B referring to Boltzmann's constant. According to Jarzynski's equation,[77] the free energy ΔA of a process equals the exponential average, $\Delta A = -k_B T \ln\langle\exp(-\Delta W/k_B T)\rangle$, of the work ΔW (which can be approximated by potential energy differences ΔE) drawn from a canonical ensemble. Of course, a sample of nine snapshots cannot be expected to provide an accurate average. Taking an exponential average results in a barrier dominated by the smallest barrier which represents the most likely path.

For further analysis of the reaction mechanism and to investigate the electrostatic influence of each single amino acid on the activation energy, the full QM density of SN-Glu-1 was replaced by electrostatically fitted charges (ESP),[78] which were fitted to reproduce the electrostatic potential of the full DFT (BP86) density polarized by the charges of the MM environment, as these can be expected to result in a quite accurate electrostatic energy at hugely reduced costs compared to the full QM density. The change in the activation energy barrier $\Delta\Delta^{\ddagger}E^i$ due to the charge on residue i can be determined as

$$\Delta\Delta^{\ddagger}E^i = \Delta^{\ddagger}E^0 - \Delta^{\ddagger}E^i \quad (2)$$

where $\Delta^{\ddagger}E^0$ is the electrostatic component of the activation energy (calculated using ESP charges instead of the QM density), and $\Delta^{\ddagger}E^i$ is the electrostatic component of the activation energy with all charges on

Table 2. Bond Distances in Å during the Reaction in SN-Glu-1

structure	N−O	N−H_N	C5′−Cγ	Hγ−Cγ	Cβ−Cα	Cγ−Cα	C5′−Cβ	Hγ−Cβ
A	2.589	1.145	3.638	1.097	1.540	2.575		
TS-**AB**	2.579	1.449	2.746	1.320	1.561	2.563		
B	2.552	1.402	3.689	2.718	1.568	2.537		
TS-**BC**	2.690	1.651			2.254	2.949		
C	2.772	1.760			3.322	3.051		
TS-**CD**	2.704	1.661			2.849	2.156		
D	2.546	1.165			2.544	1.571	4.105	3.083
TS-**DE**	2.594	1.151			2.603	1.571	2.751	1.360
E	2.552	1.160			2.578	1.555	4.180	1.096

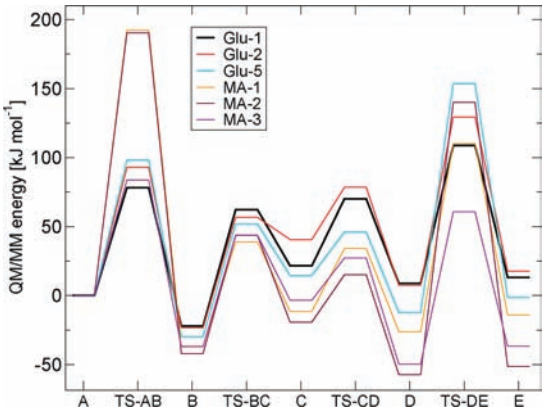

Figure 3. Energy profile, M06 at BP86 geometry (relative to **A**).

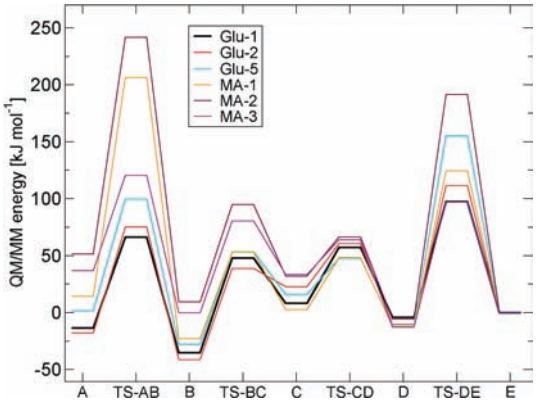

Figure 4. Energy profile, M06 at BP86 geometry (relative to **E**).

residue *i* set to 0. In these calculations, the geometries of both the reactant and the transition state (TS) are kept unchanged. Thus, the self-energy of the QM part is constant and drops out of $\Delta\Delta^{\ddagger}E^{i}$. Note that $\Delta\Delta^{\ddagger}E^{i}$ contains contributions from MM−MM interactions as well as from QM−MM interactions. If $\Delta\Delta^{\ddagger}E^{i}$ is positive, then the atom charges of residue *i* increase the barrier (destabilize the TS). Otherwise these charges stabilize the TS. $\Delta\Delta^{\ddagger}E^{i}$ estimated in this way is a semiquantitative measure of the electrostatic influence of individual residues, helpful to determine which residues play a role in the catalytic activity. However, $\Delta\Delta^{\ddagger}E^{i}$ is certainly too crude an approximation to be compared to the effect of a mutation of the respective residue on the reactivity. Among the effects not covered by $\Delta\Delta^{\ddagger}E^{i}$ are the substitution of residue *i* by other moieties and changes in the geometries as well as changes in the polarization of the QM part.

3. RESULTS AND DISCUSSION

3.1. Energy Profile of the Catalytic Reaction. The mechanism discussed in the following consists of: (1) a hydrogen transfer from glutamate substrate to Ado, (2) a rearrangement of the (*S*)-glutamyl radical to a (2*S*,3*S*)-methylaspartyl radical, and (3) a hydrogen transfer back from Ado to form the (2*S*,3*S*)-methylaspartate product. We found that the barriers for (1) and (3) dominate over the barrier of (2). Energetic data for the different elementary reactions are given in Table 1 . Relative energies were consistently calculated with respect to the energy of the state **A** obtained for the same snapshot, unless noted otherwise. Key bond distances which changed during the reaction are given in Table 2.

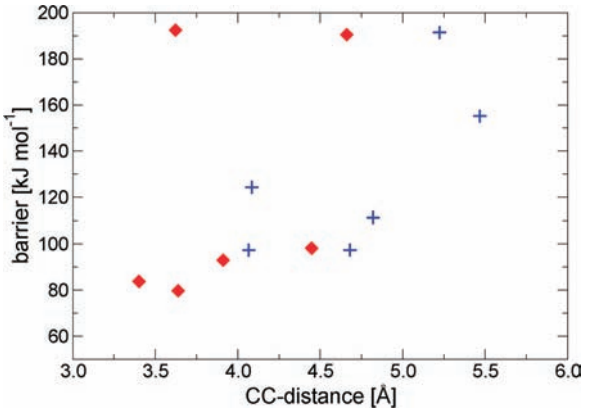

Figure 5. Barrier heights of both hydrogen transfers versus C−C-distance (C5′−Cγ for **A**, red diamonds; C5′−Cβ for **E**, blue plus signs) at energetic minima of glutamate and MA substrate (M06).

The intermediates considered in this study are labeled as follows: homolytic cleavage of the Co−C bond leads to the Ado radical and glutamate substrate, state **A**. Hydrogen transfer generates the glutamyl radical, state **B**. It fragments into acrylate and a glycyl radical, state **C**. Glycyl binding to acrylate results in the methylaspartyl radical, state **D**. At the end, the back transfer of the radical to Ado creates MA, state **E**. All transition states between the intermediates are abbreviated by TS, e.g., TS-**DE** denotes the transition state between **D** and **E**.

The barriers given in Table 1 are significantly higher for the hydrogen transfers **A** to **B** and **E** to **D** than for the rearrangement

Table 3. Energy Profiles of SN-Glu-1 with Proton Transfer Form the Substrate to the Environment Being Selectively Allowed by the Choice of the QM Part[a]

QM part	substrate + Ado + Glu 171	substrate + Ado	substrate + Ado + Glu 171 + His 150	captodative stabilization (substrate + Ado + Glu 171)
A	0.0	0.0	0.0	0.0
TS-**AB**	54.2	54.5	52.6	
B	−17.1	−14.4	−18.5	32.3
TS-**BC**	53.2	87.3	49.3	
C	30.1	76.4	28.7	14.4
TS-**CD**	61.5	87.3	61.2	
D	3.3	4.2	4.3	60.4
TS-**DE**	77.3	80.1	77.9	
E	2.6	4.4	3.8	

[a] BP86 energies in kJ mol^{-1}.

reactions **B** to **D**. There is a substantial spread in the hydrogen-transfer barriers between the different snapshots. They range from 79.7 to 192.4 kJ mol^{-1} in **A** to **B** and from 97.4 to 192.4 kJ mol^{-1} in **E** to **D**. Thus, they show a strong dependence on the environment. The smallest barriers are found in SN-Glu-1 (79.7 and 97.4 kJ mol^{-1}), suggesting that the reaction will most probably proceed via this path. SN-MA-3 and SN-Glu-1 both have a barrier height of 97.4 kJ mol^{-1} for the transition **E** to **D**. However, the barrier for **A** to **B** is slightly lower (74.7 kJ mol^{-1}) in SN-Glu-1 than in SN-MA-3 (83.8 kJ mol^{-1}). Accordingly, further investigation of the protein will mainly be performed with SN-Glu-1. The exponentially averaged barrier at T = 300 K is 84.8 kJ mol^{-1} for **A** to **B** and 101.1 kJ mol^{-1} for **E** to **D**.

The barriers for hydrogen transfer and recombination of the fragments seem to depend stronger on the snapshot than the barriers for the fragmentation (see Figures 3 and 4). Thus, the hydrogen-transfer reactions depend much more on the enzyme environment than the carbon skeleton rearrangement.

The exponential average is smaller with 84.8 kJ mol^{-1} for the reaction **A** to **B** than for **E** to **D** with 101.1 kJ mol^{-1}. The lowest barriers contribute most to the exponential average. So, a similar difference is obtained when just comparing the lowest values for the two mechanisms: 79.7 kJ mol^{-1} for the former and 97.4 kJ mol^{-1} for the latter case. For coenzyme B_{12}-dependent diol dehydratase, an enzyme similar to GM, the rate-limiting step was predicted[16] to exhibit a barrier between 60 and 75 kJ mol^{-1} based on theoretical and experimental studies.[79−81] In GM, we find the barrier to be about 25 kJ mol^{-1} higher.

The wide range of barriers found in the different snapshots is due to the varying geometries of the snapshots. Differences will be discussed in more detail in Section 3.3. Comparison of the reaction **B** to **D** in Figures 3 and 4 leads to the insight that the barriers from **B** to **C** (average: 80.1 kJ mol^{-1}) as well as the barriers from **D** to **C** (average: 62.4 kJ mol^{-1}) are about the same height in all snapshots. The influence of the protein on the carbon skeleton rearrangement will be discussed in Section 3.2.

Figure 5 shows the barriers versus the C−C distance between the hydrogen donor and acceptor in **A** and **E**. Independent of the snapshots and of the substrate in the binding pocket at the beginning of the simulations, **A** tends to have shorter distances than **D**. Distances refer to the minimum structure. In many cases the distance can be decreased without significantly increasing the energy. Promoting vibrations may lead to shorter hydrogen-transfer distances. The large distances (>5 Å) are associated with large barriers. The reaction will not proceed via these paths. SN-Glu-3, SN-Glu-4, and SN-Glu-6 show significantly higher barriers than the other snapshots already with the BP86 functional (which underestimates the barrier heights). Thus, these snapshots have not been investigated in more detail, see Figure S3 of the Supporting Information. In one case a large barrier is found for a short distance. In the respective snapshot (SN-Glu-3) one catalytic hydrogen bond is broken, see Section 3.3, which causes the large barrier.

Table 4. Relative Energies of the Isolated Substrate Radical Optimized in the Gas Phase and in Water (COSMO) (kJ mol^{-1})

	gas phase		COSMO
	G3(MP2)-RAD(p)[16]	BP86	BP86
B	0.0	0.0	0.0
TS-**BC**	59.9	69.9	69.1
C	34.4	2.8	3.6
TS-**CD**	66.5	78.0	84.2
D	20.3	24.9	31.1

3.1.1. Catalytic Role of Glu 171. The side chain of Glu 171 is positioned next to the ammonium group (NH_3^+) of the glutamate substrate. During the fragmentation−recombination process, a proton is transferred from the ammonium group to Glu 171 in all snapshots, see Figure 2. In our simulations transfer of protons between the QM part and the MM part is impossible. Thus, the inclusion of neighboring amino acids in the QM part allows such acid−base reactions to take place, whereas the exclusion prevents them. The barriers of the rearrangement of the carbon skeleton are about 30−40 kJ mol^{-1} higher if the proton transfer to Glu 171 is forbidden by the choice of the QM-part in SN-Glu-1, which has the lowest hydrogen-transfer barriers, see Table 3. This is in agreement with mutation studies in which Glu 171 was replaced by Gln and other amino acids. These show a dramatic decrease in reactivity, and, thus, the importance of Glu 171.[10] Further investigations including His 150 in the QM part showed that His 150 does not act as a proton acceptor.

A captodative stabilization, i.e., a proton transfer from the ammonium group to the carboxyl group of the glycyl radical in **C** was proposed by gas-phase calculations.[16] This is energetically unfavorable by about 50, 15, and 60 kJ mol^{-1} for **B**, **C**, and **D**, respectively, in a QM/MM environment (SN-Glu-1), see Table 3 columns 2 and 5. The protein stabilizes the zwitterionic state.

3.2. Catalytic Effect of the Protein. Variation in the protein environment has a significant influence on the energy barriers for the hydrogen transfers. This causes a large spread in the barriers between the snapshots (Figures 3 and 4). The reaction will predominantly proceed via the paths with the lowest barriers.

Intermediate **B**, containing the glutamyl radical, is the most stable structure along the part of the reaction path under study, in agreement with experimental results.[20] In all calculations, in protein as well as in gas phase and in water, **B** has the lowest energy along the reaction path.

The barrier for fragmentation is similar in the gas phase (69.9 kJ mol^{-1}), in water (69.1 kJ mol^{-1}), Table 4, and in the protein (70.1 kJ mol^{-1}) for calculations with BP86 functional.

Table 5. Residues of the Environment with an Electrostatic Influence on the Activation Barrier of $|\Delta\Delta^{\ddagger}E^{i}| > 3$ kJ mol^{-1} in Either TS-AB or TS-DE (SN-Glu-1)

		$\Delta\Delta^{\ddagger}E^{i}$ (kJ mol^{-1})	
residue	charge	**A** to **B**	**D** to **E**
σ Subunit			
Asp 14	−1	0.2	−3.4
His 16	0	−3.7	−8.2
cobalamin	0	−7.0	−6.7
ε Subunit			
Arg 66	+1	−3.7	3.2
Arg 100	+1	−4.7	−1.2
Gln 147	0	3.2	0.7
Arg 149	+1	2.4	6.2
His 150	0	10.9	−1.2
Tyr 177	0	10.5	−1.7
Asp 198	−1	−4.9	−-1.1
Arg 213	+1	7.3	2.0
Glu 214	−1	−14.5	−5.8
Phe 216	0	4.4	−0.2
Glu 236	−1	−4.8	−1.6
Met 294	0	1.1	3.0
Lys 322	+1	8.4	2.9
Lys 326	+1	−8.2	−2.6
Glu 330	−1	13.9	12.2
water 632	0	3.9	6.0
water 635	0	−0.5	−3.0
water 637	0	−6.6	−6.8
water 642	0	3.4	4.2
water 648	0	3.9	2.5
water 654	0	−5.3	−7.5

The rearrangement of the carbon skeleton is less influenced by the protein environment than the hydrogen transfers. All snapshots show barriers within 75.9 and 82.9 kJ mol^{-1} for the fragmentation (**B** to **C**) and within 30.6 and 49.2 kJ mol^{-1} for the recombination (**C** to **D**), see Table 1.

The enantioselective catalysis by suppressing the formation of the (*R*)-enantiomer happens in step **C** to **D**.

The C−C rearrangement is hardly influenced by a water environment compared to gas-phase calculations. Comparison of the energies of the substrate in the enzyme environment, water (COSMO), and the gas phase is given in Table 4 . The enzyme sterically destabilizes the fragments (state **C**). **C** is about as stable as **B** in water or the gas phase, see Table 4, while it is 43.3 kJ mol^{-1} (see Table 1, which gives the M06 values; the BP86 value is 47.1 kJ mol^{-1}) less stable in the enzyme. **C** is destabilized predominantly sterically. This reduces the barriers to recombine the fragments (**C** to **D**) from 75.2 kJ mol^{-1} in the gas phase and 80.6 kJ mol^{-1} in water down to 31.4 kJ mol^{-1} (all BP86) in the enzyme environment. In gas phase and water the fragments lie parallel to each other, while in the enzyme environment they are rotated and in a staggered position. The two fragments are held in place by the enzyme environment: The arginine claw prevents the fragments acrylate and glycyl to move into a parallel position. This raises the energy of the intermediate **C** but avoids the rotation of the acrylate and, thus, ensures the enantioselectivity. Additionally, the formation of a bond between glycyl and the acrylate is facilitated.

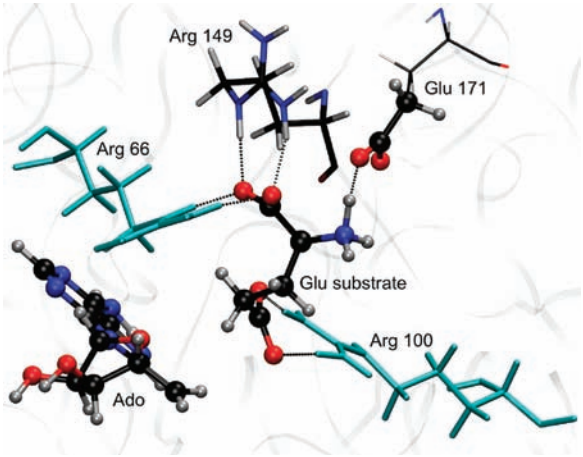

Figure 6. Arginine claw of the glutamate substrate (intermediate **A**). Residues with $7 > |\Delta\Delta^{\ddagger}E^{i}| > 3$ kJ mol^{-1} are shown in cyan. They stabilize the transition state. Additionally, the QM part comprising Ado, the glutamate substrate, and Glu 171 is shown (ball-and-stick).

Table 4 compares the reaction energies of isolated glutamate in the gas phase and in water (COSMO) at different levels of theory. Compared to the G3(MP2)-RAD(p) level at a different protonation state,[16] calculations with BP86 result in a larger barrier. The reaction of the isolated glutamate in the gas phase is overall endothermic (Table 4). The enzyme can save this intrinsic energy for the last step of the reaction.

3.3. Influence of Individual Residues on the Reactivity. After having located the transition and reactant states connected to them, we estimated the electrostatic influence of individual residues (neighboring amino acids and water molecules) on the activation barriers using static structures.

The resulting values for $\Delta\Delta^{\ddagger}E^{i}$ both for the reactions **A** to **B** and **D** to **E** are given in Table 5. The residues with larger values of $\Delta\Delta^{\ddagger}E^{i}$ are depicted in Figures 6−9. In the following, individual amino acids and their influence on the reactivity will be discussed, first for the reaction **A** to **B** and then for **D** to **E**. Throughout this manuscript, hydrogen-bond distances are given between the hydrogen and heavy atoms (acceptor).

3.3.1. Arginine Claw. Arg 66, 100, and 149 form the arginine claw, see Figure 6. Arg 100 builds a salt bridge to the carboxyl group of the side chain of the glutamate substrate, while Arg 66 and Arg 149 are bound to its "backbone" carboxyl group (which is not, in fact, a part of any protein backbone, we refer here to the carboxyl group bound to the Cα atom). Since each arginine donates two hydrogen bonds, a total of six such bonds make up the arginine claw. Their electrostatic effect on the barriers for hydrogen transfer is moderate, see Table 5 . This is mainly due to the fact that the interaction between the substrate and the arginine claw is hardly altered during the mechanism in the snapshot for which the electrostatic contributions were calculated (SN-Glu-1). A slight tightening of the arginine claw is observed during the fragmentation. Qualitatively the same behavior is observed for SN-Glu-2 and SN-Glu-5.

During the hydrogen-transfer reactions, the glutamate substrate moves slightly toward Ado, which means it moves away from Arg 149. Consequently, in two snapshots (SN-MA-1 and

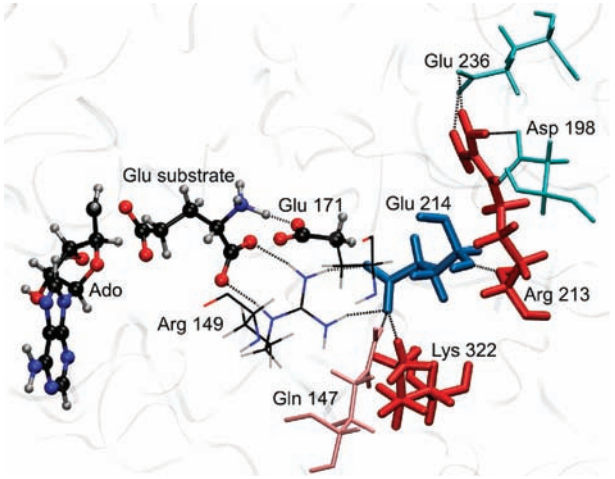

Figure 7. Environment of the glutamate substrate (intermediate **A**). Residues with $|\Delta\Delta^{\ddagger}E^{i}| > 7$ kJ mol^{-1} are shown as thicker sticks with darker colors. Thinner sticks and lighter colors denote residues with $7 > |\Delta\Delta^{\ddagger}E^{i}| > 3$ kJ mol^{-1}. Additionally, the QM part comprising Ado, the glutamate substrate, and Glu 171 is shown (ball-and-stick). Residues shown in blue stabilize the transition state, and residues shown in red destabilize the transition state with respect to the resting state.

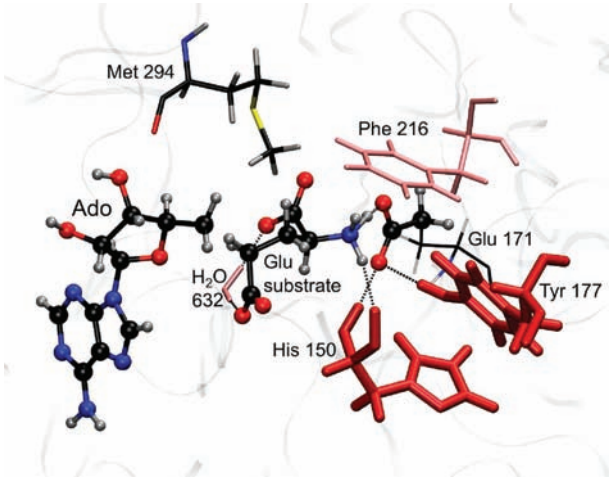

Figure 8. Environment of Glu 171 (intermediate **A**). See Figure 7 for details. Residues with $|\Delta\Delta^{\ddagger}E^{i}| > 7$ kJ mol^{-1} are shown as thicker sticks with darker colors. Thinner sticks and lighter colors denote residues with $7 > |\Delta\Delta^{\ddagger}E^{i}| > 3$ kJ mol^{-1}. Additionally, the QM part comprising Ado, the glutamate substrate, and Glu 171 is shown (ball-and-stick). Residues shown in red destabilize the transition state with respect to the resting state.

SN-MA-3) Arg 149 forms one hydrogen bond to the carboxyl group of Glu 171, while one to the substrate is absent in the structure derived from the MD simulation (**E**). The other hydrogen bond between Arg 149 is stable in those cases, though. During the reaction mechanism also the second hydrogen bond establishes.

In one snapshot (SN-Glu-3), the arginine claw is opened even further. Only one hydrogen bond between Arg 100 and glutamate remains stable, the other one is broken. This particular snapshot shows the highest energies of the intermediates TS-**BC** to **E**, about 50 kJ mol^{-1} higher than in the other snapshots, on a BP86 level. This can be interpreted as a clear indication that an intact arginine claw is crucial for the catalytic activity.

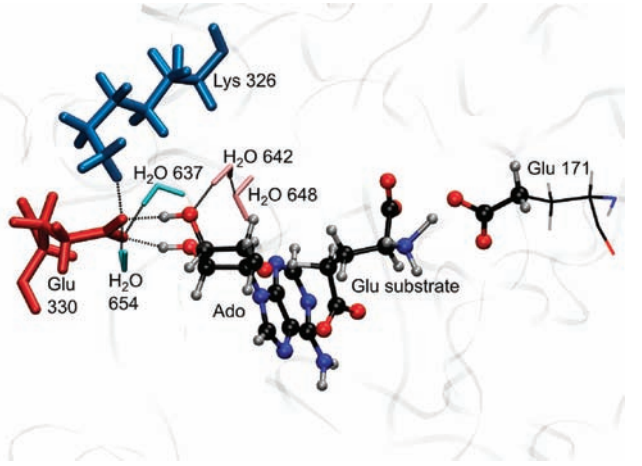

Figure 9. Environment of Ado (intermediate **A**). See Figure 7 for details. Residues with $|\Delta\Delta^{\ddagger}E^{i}| > 7$ kJ mol^{-1} are shown as thicker sticks with darker colors. Thinner sticks and lighter colors denote residues with $7 > |\Delta\Delta^{\ddagger}E^{i}| > 3$ kJ mol^{-1}. Additionally, the QM-part comprising Ado, the glutamate substrate, and Glu 171 is shown (ball-and-stick). Residues shown in blue stabilize the transition state, and residues shown in red destabilize the transition state with respect to the resting state.

Table 6. Difference of the Dihedral Cβ−Cγ−Sδ−Cε of Met 294 in Different Snapshots Compared to Intermediate A To Describe the Movement of the Methyl Group of Met 294 Located Between Ado and the Glutamate Substrate

	SN-Glu-1	SN-Glu-2	SN-Glu-3	SN-Glu-5
A	0	0	0	0
TS-AB	7.2	1.2	−2.1	0.4
B	−0.8	0.5	−0.4	−0.2
TS-BC	−2.4	0.9	0.2	2.1
C	−10.4	−0.9	−0.6	1.5
TS-CD	−10.5	−0.3	3.9	2.2
D	−5.0	0.8	3.3	1.8
TS-DE	−2.2	0.4	3.7	3.7
E	−4.3	−0.7	3.4	2.5
	SN-MA-1	**SN-MA-2**		**SN-MA-3**
A	0	0		0
TS-AB	−1.0	−0.2		0.9
B	0.5	−0.1		0.7
TS-BC	−0.1	0.0		1.3
C	−0.6	0.8		2.7
TS-CD	−1.1	−0.6		2.6
D	−1.6	−0.1		0.5
TS-DE	−2.6	−5.4		0.3
E	−1.3	0.3		−0.0

3.3.2. Environment of the Glutamate Substrate. Here we discuss the residues Arg 213, Glu 214, Lys 322, and Gln 147, connected to the glutamate substrate via Arg 149 (which is part of the arginine claw), see Figure 7 . In the reaction from **A** to **B** a proton is transferred form the glutamate substrate to Glu 171. Its charge changes from −1 to 0. The dipole moment of the whole reactive center changes. Thus, negatively charged residues (Glu 214, Glu 236, and Asp 198) in the vicinity of Glu 171 stabilize the

transition state, while positive ones (Lys 322 and Arg 213) destabilize it. Despite their large distance, these residues seem to have a significant electrostatic influence on the reaction. For example Lys 322 is 8 Å (closest atom) away from the transferred proton and increases the barrier by 8.4 kJ mol^{-1}, see Table 5 . Glu 214 is 5.2 Å away (4.9 Å in TS-**AB**) and decreases the barrier by 14.5 kJ mol^{-1}. In **D** the proton is already back at the substrate, so the above-mentioned residues have a weaker effect on the barrier from **D** to **E**.

Tyr 177 provides a hydrogen bond to Glu 171 via its phenol group, see Figure 8. This bond is elongated during the reaction from **A** to **B** which destabilizes the transition state in SN-Glu-1. This is in contrast to the other snapshots where that hydrogen bond is hardly altered in the steps **A** to **B** and **D** to **E**.

His 150 provides a hydrogen bond via its backbone oxygen to a proton of the ammonium group of the glutamate substrate, see Figure 8 . The bond is present in SN-Glu-1 and SN-MA-2 and absent (>2.2 Å) in the other snapshots. In both, SN-Glu-1 and SN-MA-2, the hydrogen bond elongates during the carbon skeleton rearrangement.

3.3.3. Environment of Ado. Glu 330, Lys 326 and four water molecules change their bonding pattern to Ado during the hydrogen-transfer reactions. The carboxyl side chain of Glu 330 accepts a hydrogen bond from each of the two OH-groups of the ribose ring. In some of the snapshots (SN-MA-2, SN-Glu-2, SN-Glu5) one of these hydrogen bonds opens during the transitions **A** to **B** and **D** to **E**. In SN-MA-1 one of the bonds is open in structures **A** to **C**, resulting in a large barrier (192.4 kJ mol^{-1}) for hydrogen transfer and closed in the further structures. In summary, in the snapshots with the lowest barriers (SN-Glu-1 and SN-MA-3) both hydrogen bonds between Glu 330 and the ribose ring remain stable (see Figure 9).

Glu 330 was found to destabilize TS-**AB** by 13.9 kJ mol^{-1} and TS-**DE** by 12.2 kJ mol^{-1}. Lys 326 stabilizes TS-**AB** by 8.2 kJ mol^{-1} but stabilizes TS-**DE** by only 2.6 kJ mol^{-1}. Two water molecules (water 654 and 637) stabilize TS-**AB** by more than 3 kJ mol^{-1} through shortening their hydrogen bonds to Glu 330. Another water molecule (642) increases the barrier by 3.4 kJ mol^{-1} by elongating its hydrogen bond to one OH-group of the ribose ring in Ado.

3.3.4. Met 294. The side chain of Met 294 has to move to enable the hydrogen transfer from Ado to the substrate and back, see Figure 8. That requires energy and, thus, increases the barrier. It plays a more important role in **D** to **E** where it increases the barrier by 3 kJ mol^{-1}, than in **A** to **B**. Table 6 shows a dihedral angle in Met 294 that indicates the movement of a methyl group located between the substrate and Ado. The strongest movement is found in SN-Glu-1, which has the lowest barriers for the hydrogen transfers. Noteworthy, Met 294 is not in direct contact with the reactive center, but it influences the reaction barriers.

4. CONCLUSIONS

We study the reaction mechanism of glutamate mutase in atomistic detail using the QM/MM approach. The conversion of glutamate to methylaspartate proceeds via a fragmentation−recombination mechanism. The enzymatic reaction is compared to the uncatalyzed reaction in water and in the gas phase. We identify the hydrogen transfers as rate limiting steps. With a barrier of 101.1 kJ mol^{-1} the transfer **E** to **D** is found to be rate limiting. However, the barrier from **A** to **B** is similar with 84.8 kJ mol^{-1}.

The enzyme environment has a stronger impact on the hydrogen transfers **A** to **B** and **D** to **E** than on the carbon skeleton rearrangement **B** to **D**. The influence is mostly electrostatical and to a lesser degree sterical.

Glu 171, in the vicinity of the glutamate substrate, acts as a catalytic residue by temporarily abstracting a proton from the ammonium group of the substrate. This facilitates the carbon skeleton rearrangement steps (**B** to **D**). The proton-transfer changes the dipole moment of the whole active site, an effect being electrostatically buffered by the protein environment.

The arginine claw (Arg 66, Arg 100, and Arg 149) keeps the intermediate fragments in place. It raises the energy of intermediate **C** by steric effects and, thus, facilitates the recombination process. We find that an open arginine claw leads to much higher energies of the intermediates, whereas a closed arginine claw is associated with reaction paths exhibiting the lowest reaction barriers. The arginine claw is crucial for a successful catalysis.

We find significant catalytic roles of the amino acids Glu 214, Lys 322, Gln 147, Glu 330, Lys 326, and Met 294. During the hydrogen transfer Glu 330 reduces the barrier by establishing stable hydrogen bonds to the ribose ring of Ado. Our careful investigation of the enzyme environment of the active center lead to the identification of additional residues important for the reaction. These results highlight new promising experimental targets. We find amino acids in considerable distance to the active center to have a noticeable influence on the reaction.

■ ASSOCIATED CONTENT

Supporting Information. Calculational details (PDF), force field parameters for cobalamin and MA, a reaction path with all stationary geometries of SN-Glu-1 (pdb), and complete refs 26, 41, and 63. This material is available free of charge via the Internet at http://pubs.acs.org.

■ AUTHOR INFORMATION

Corresponding Author
*E-mail: kaestner@theochem.uni-stuttgart.de.

■ ACKNOWLEDGMENT

The authors thank the German Research Foundation (DFG) for financial support of the project within the Cluster of Excellence in Simulation Technology (EXC 310/1) at the University of Stuttgart. Prof. E. N. G. Marsh is acknowledged for helpful discussions.

■ REFERENCES

(1) Brunold, T.; Conrad, K.; Liptak, M.; Park, K. *Coord. Chem. Rev.* **2009**, *253*, 779.
(2) Gruber, K.; Kratky, C. *Curr. Opin. Chem. Biol.* **2002**, *6*, 598.
(3) Buckel, W. *Appl. Microbiol. Biotechnol.* **2001**, *57*, 263.
(4) Reitzer, R.; Gruber, K.; Jogl, G.; Wagner, U.; Bothe, H.; Buckel, W.; Kratky, C. *Structure* **1999**, *7*, 891.
(5) Gruber, K.; Reitzer, R.; Kratky, C. *Angew. Chem., Int. Ed. Engl.* **2001**, *40*, 3377.
(6) Tollinger, M.; Konrat, R.; Hilbert, B.; Marsh, E. N. G.; Kräutler, B. *Structure* **1998**, *6*, 1021.
(7) Hoffmann, B.; Konrat, R.; Bothe, H.; Buckel, W.; Kräutler, B. *Eur. J. Biochem.* **1999**, *263*, 178.
(8) Tollinger, M.; Eichmüller, C.; Konrat, R.; Huhta, M.; Marsh, E. N. G.; Kräutler, B. *J. Mol. Biol.* **2001**, *309*, 777.

(9) Hoffmann, B.; Tollinger, M.; Konrat, R.; Huhta, M.; Marsh, E. N. G.; Kräutler, B. *ChemBioChem* **2001**, *2*, 643.
(10) Marsh, E. N. G.; Madhavapeddi, P. *Chem. Biol.* **2001**, *8*, 1143.
(11) Marsh, E. N. G. *Bioorg. Chem.* **2000**, *28*, 176.
(12) Buckel, W.; Golding, B. T. *Chem. Soc. Rev.* **1996**, *25*, 329.
(13) Jensen, K.; Ryde, U. *Coord. Chem. Rev.* **2009**, *253*, 769.
(14) Jensen, K.; Ryde, U. *J. Am. Chem. Soc.* **2005**, *127*, 9117.
(15) Kozlowski, P. *Curr. Opin. Chem. Biol.* **2001**, *5*, 736.
(16) Wetmore, S. D.; Smith, D. M.; Golding, B. T.; Radom, L. *J. Am. Chem. Soc.* **2001**, *123*, 7963.
(17) Chih, H.-W.; Marsh, E. N. G. *J. Am. Chem. Soc.* **2000**, *122*, 10732.
(18) Marsh, E. N. G.; Patwardhan, A. *Arch. Biochem. Biophys.* **2007**, *461*, 194.
(19) Cheng, M.-C.; Marsh, E. N. G. *Biochemistry* **2005**, *44*, 2686.
(20) Chih, H.-W.; Marsh, E. N. G. *Biochemistry* **2001**, *40*, 13060.
(21) Marsh, E. N. G.; Ballou, D. P. *Biochemistry* **1998**, *37*, 11864.
(22) Yoon, M.; Kalli, A.; Lee, H.-Y.; Håkansson, K.; Marsh, E. N. G. *Angew. Chem., Int. Ed.* **2007**, *46*, 8455.
(23) Yoon, M.; Song, H.; Håkansson, K.; Marsh, E. N. G. *Biochemistry* **2010**, *49*, 3168.
(24) Warshel, A.; Karplus, M. *J. Am. Chem. Soc.* **1972**, *94*, 5612.
(25) Warshel, A.; Levitt, M. *J. Mol. Biol.* **1976**, *103*, 227.
(26) Sherwood, P.; et al. *J. Mol. Struct. (Theochem.)* **2003**, *632*, 1.
(27) Senn, H.; Thiel, W. *Topics in Current Chemistry*; Springer: Berlin, Germany, 2007; Vol. 268, p 173.
(28) Senn, H.; Thiel, W. *Curr. Op. Chem. Biol.* **2007**, *11*, 182.
(29) Lin, H.; Truhlar, D. *Theor. Chem. Acc.* **2007**, *117*, 185.
(30) Riccardi, D.; Schaefer, P.; Yang, Y.; Yu, H.; Ghosh, N.; Prat-Resina, X.; Knig, P.; Li, G.; Xu, D.; Guo, H.; Elstner, M.; Cui, Q. *J. Phys. Chem. B* **2006**, *110*, 6458.
(31) Chowdhury, S.; Banerjee, R. *Biochemistry* **2000**, *39*, 7998.
(32) Sandala, G. M.; Smith, D. M.; Marsh, E. N. G.; Radom, L. *J. Am. Chem. Soc.* **2007**, *129*, 1623.
(33) Li, X.; Chung, L. W.; Paneth, P.; Morokuma, K. *J. Am. Chem. Soc.* **2009**, *131*, 5115.
(34) Dybala-Defratyka, A.; Paneth, P.; Banerjee, R.; Truhlar, D. G. *Proc. Natl. Acad. Sci. U.S.A.* **2007**, *104*, 10774.
(35) Loferer, M. J.; Webb, B. M.; Grant, G. H.; Liedl, K. R. *J. Am. Chem. Soc.* **2003**, *125*, 1072.
(36) Padmakumar, R.; Padmakumar, R.; Banerjee, R. *Biochemistry* **1997**, *36*, 3713–3718.
(37) Mancia, F.; Keep, N. H.; Nakagawa, A.; Leadlay, P. F.; S., M.; Rasmussen, B.; Bosecke, P.; Diat, O.; Evans, P. R. *Structure* **1996**, *4*, 339.
(38) Chen, H.-P.; Marsh, E. N. G. *Biochemistry* **1997**, *36*, 14939.
(39) Humphrey, W.; Dalke, A.; Schulten, K. *J. Mol. Graphics* **1996**, *14*, 33.
(40) Jorgensen, W.; Chandrasekhar, J.; Madura, J.; Impey, R.; Klein, M. *J. Chem. Phys.* **1983**, *79*, 926.
(41) MacKerell, A. D., Jr.; et al. *J. Phys. Chem. B* **1998**, *102*, 3586.
(42) MacKerell, A. D., Jr.; Feig, M.; Brooks, C. L., III *J. Comput. Chem.* **2004**, *25*, 1400.
(43) Foloppe, N.; MacKerell, A. D., Jr. *J. Comput. Chem.* **2000**, *21*, 86.
(44) MacKerell, A., Jr.; Banavali, N. *J. Comput. Chem.* **2000**, *21*, 105.
(45) Phillips, J.; Braun, R.; Wang, W.; Gumbart, J.; Tajkhorshid, E.; Villa, E.; Chipot, C.; Skeel, R.; Kale, L.; Schulten, K. *J. Comput. Chem.* **2005**, *26*, 1781.
(46) Tuckerman, M. E.; Berne, B. J.; Martyna, G. J.; L., K. M. *J. Chem. Phys.* **1993**, *99*, 2796.
(47) Feller, S.; Zhang, Y.; Pastor, R.; Brooks, B. *J. Chem. Phys.* **1995**, *103*, 4613.
(48) Hohenberg, P.; Kohn, W. *Phys. Rev. B* **1964**, *136*, 864.
(49) Kohn, W.; Sham, L. *Phys. Rev. A* **1965**, *140*, 1133.
(50) de Vries, A. H.; Sherwood, P.; Collins, S. J.; Rigby, A. M.; Rigutto, M.; Kramer, G. J. *J. Phys. Chem. B* **1999**, *103*, 6133.
(51) Smith, W.; Yong, C.; Rodger, P. *Mol. Simul.* **2002**, *28*, 385.
(52) Dirac, P. *Proc. R. Soc. London, Ser. A* **1929**, *123*, 714.
(53) Slater, J. *Phys. Rev.* **1951**, *81*, 385.
(54) Vosko, S. H.; Wilk, L.; Nusair, M. *Can. J. Phys.* **1980**, *58*, 1200.
(55) Becke, A. *Phys. Rev. A* **1988**, *38*, 3098.
(56) Perdew, J. *Phys. Rev. B* **1986**, *33*, 8822.
(57) Grimme, S. *J. Comput. Chem.* **2004**, *25*, 1463.
(58) Stephens, P. J.; Devlin, F. J.; Chabalowski, C. F.; Frisch, M. J. *J. Phys. Chem.* **1994**, *98*, 11623.
(59) *TURBOMOLE*, v 6.0.2; TURBOMOLE GmbH: Karlsruhe, Germany, 2009; http://www.turbomole.com.
(60) Arnim, M. v.; Ahlrichs, R. *J. Comput. Chem.* **1998**, *19*, 1746.
(61) Zhao, Y.; Truhlar, D. G. *J. Chem. Phys.* **2006**, *125*, 194101.
(62) Kendal, R. A.; Apra, E.; Bernholdt, D. E.; Bylaska, E. J.; Dupuis, M.; Fann, G. I.; Harrison, R. J.; Ju, J.; Nichols, J. A.; Nieplocha, J.; Straatsma, T. P.; Windus, T. L.; Wong, A. T. *Comput. Phys. Commun.* **2000**, *128*, 260.
(63) Bylaska, E. J. et al. *NWChem, A Computational Chemistry Package for Parallel Computers*, version 5.1; Pacific Northwest National Laboratory, Richland, Washington, Technical Report, 2007.
(64) Zhao, Y.; Truhlar, D. G. *Theor. Chem. Acc.* **2008**, *120*, 215.
(65) Schäfer, A.; Horn, H.; Ahlrichs, R. *J. Chem. Phys.* **1992**, *97*, 2571.
(66) Dunning, T. *J. Chem. Phys.* **1989**, *90*, 1007.
(67) Weigend, F.; Häser, M.; Patzelt, H.; Ahlrichs, R. *Chem. Phys. Lett.* **1998**, *294*, 143.
(68) Kästner, J.; Carr, J. M.; Keal, T. W.; Thiel, W.; Wander, A.; Sherwood, P. *J. Phys. Chem. A* **2009**, *113*, 11856.
(69) Billeter, S. R.; Turner, A. J.; Thiel, W. *Phys. Chem. Chem. Phys.* **2000**, *2*, 2177.
(70) Kästner, J.; Sherwood, P. *J. Chem. Phys.* **2008**, *128*, 014106.
(71) Henkelman, G.; Jónsson, H. *J. Chem. Phys.* **1999**, *111*, 7010.
(72) Olsen, R. A.; Kroes, G. J.; Henkelman, G.; Arnaldsson, A.; Jónsson, H. *J. Chem. Phys.* **2004**, *121*, 9776.
(73) Heyden, A.; Bell, A. T.; Keil, F. J. *J. Chem. Phys.* **2005**, *123*, 224101.
(74) Klamt, A.; Schüürmann, G. *J. Chem. Soc., Perkin Trans.* **1993**, *2*, 799.
(75) Kästner, J.; Sherwood, P. *Mol. Phys.* **2010**, *108*, 293.
(76) Lonsdale, R.; Harvey, J. N.; Mulholland, A. J. *J. Phys. Chem. B* **2010**, *114*, 1156.
(77) Jarzynski, C. *Phys. Rev. Lett.* **1997**, *78*, 2690.
(78) Bayly, C.; Cieplak, P.; Cornell, W.; Kollman, P. *J. Phys. Chem.* **1993**, *97*, 10269.
(79) Smith, D. M.; Golding, B. T.; Radom, L. *J. Am. Chem. Soc.* **1999**, *121*, 1383.
(80) Smith, D. M.; Golding, B. T.; Radom, L. *J. Am. Chem. Soc.* **2001**, *123*, 1664.
(81) George, P.; Glusker, J.; Bock, C. *J. Am. Chem. Soc.* **1997**, *119*, 7065.